BIOCHEMISTRY
including biophysical chemistry & molecular biology
Article

Biochemistry **2011,** *50,* 1885–1893 1885
DOI: 10.1021/bi101921w

A High-Affinity Adenosine Kinase from *Anopheles gambiae*†

María B. Cassera, Meng-Chiao Ho, Emilio F. Merino, Emmanuel S. Burgos, Agnes Rinaldo-Matthis,‡ Steven C. Almo, and Vern L. Schramm*

Department of Biochemistry, Albert Einstein College of Medicine, Yeshiva University, Bronx, New York 10461, United States.
‡Present address: Department of Medical Biochemistry and Biophysics, Division of Chemistry II, Karolinska Institutet, S-171 77 Stockholm, Sweden.

Received December 1, 2010; Revised Manuscript Received January 12, 2011

ABSTRACT: Genome analysis revealed a mosquito orthologue of adenosine kinase in *Anopheles gambiae* (*Ag*AK; the most important vector for the transmission of *Plasmodium falciparum* in Africa). *P. falciparum* are purine auxotrophs and do not express an adenosine kinase but rely on their hosts for purines. *Ag*AK was kinetically characterized and found to have the highest affinity for adenosine (K_m = 8.1 nM) of any known adenosine kinase. *Ag*AK is specific for adenosine at the nucleoside site, but several nucleotide triphosphate phosphoryl donors are tolerated. The *Ag*AK crystal structure with a bound bisubstrate analogue Ap_4A (2.0 Å resolution) reveals interactions for adenosine and ATP and the geometry for phosphoryl transfer. The polyphosphate charge is partly neutralized by a bound Mg^{2+} ion and an ion pair to a catalytic site Arg. The *Ag*AK structure consists of a large catalytic core in a three-layer α/β/α sandwich, and a small cap domain in contact with adenosine. The specificity and tight binding for adenosine arise from hydrogen bond interactions of Asn14, Leu16, Leu40, Leu133, Leu168, Phe168, and Thr171 and the backbone of Ile39 and Phe168 with the adenine ring as well as through hydrogen bond interactions between Asp18, Gly64, and Asn68 and the ribosyl 2′- and 3′-hydroxyl groups. The structure is more similar to that of human adenosine kinase (48% identical) than to that of AK from *Toxoplasma gondii* (31% identical). With this extraordinary affinity for *Ag*AK, adenosine is efficiently captured and converted to AMP at near the diffusion limit, suggesting an important role for this enzyme in the maintenance of the adenine nucleotide pool. mRNA analysis verifies that *Ag*AK transcripts are produced in the adult insects.

Anopheles gambiae is the most important malaria vector in Africa, responsible for the transmission of *Plasmodium falciparum*. Malaria is a leading cause of illness and death in the tropics, with 300−500 million clinical cases and more than 1 million deaths per year (*1*). *P. falciparum* is a purine auxotroph, salvaging host cell purines for synthesis of cofactors and nucleic acids (*2*, *3*). Parasite cell growth and division demands robust purine salvage, in particular adenosine, because the parasite contains the most (A+T)-rich genome sequenced to date (approximately 80%). Adenosine metabolism has been well characterized during *P. falciparum* growth in the erythrocytic stages (*4*) but not in the mosquito vector. Human AK uses adenosine efficiently (K_m = 41 nM) but is inhibited when the concentration is high, thus preventing excess accumulation of intracellular purine nucleotides (*5*). Adenosine kinase (EC 2.7.1.20) catalyzes the phosphorylation of adenosine using $MgATP^{2-}$ as the phosphoryl donor to release AMP[1] and adenosine 5′-diphosphate (ADP). Most studies of this enzyme have been directed toward inhibitor design, especially in parasitic protozoa, bacteria, and humans (*6*−*11*). Adenosine kinases have been purified from human, yeast, and protozoa and extensively characterized at kinetic and structural levels. Sequence analysis has shown that human adenosine kinase has similarities to microbial ribokinases and fructokinases from the phosphofructokinase B type (PFK-B) family (*5*, *12*). Despite the common feature of ATP-binding sites, these kinases have different functions and share a low overall degree of sequence identity (∼20%), preventing precise determination of the structural and functional characteristics of new members.

Purine metabolism in *Anopheles* spp. remains poorly explored. Characterization and understanding of mosquito purine metabolism might identify new targets for specific insecticides to control this malaria vector and to facilitate study of purine metabolism in the mosquito and in the malaria parasite in the sexual stages. Purine metabolism in *A. gambiae* mosquitoes can be predicted through the genome sequence (*13*), allowing *in silico* comparison of parasite, vector, and human metabolism. Anopheline genome analysis revealed a mosquito orthologue of adenosine kinase (*Ag*AK). The anopheline AK was expressed, kinetically characterized, and found to exhibit the lowest K_m known for any adenosine kinase and to be genetically expressed in the insect by direct mRNA analysis. Crystallographic analysis

†This work was supported by National Institutes of Health Grant AI049512.

*To whom correspondence should be addressed: Department of Biochemistry, Albert Einstein College of Medicine, 1300 Morris Park Ave., Bronx, NY 10461. Telephone: (718) 430-2813. Fax: (718) 430-8565. E-mail: vern.schramm@einstein.yu.edu.

[1]Abbreviations: AMP, adenosine 5′-monophosphate; GTP, guanosine 5′-triphosphate; UTP, uridine 5′-triphosphate; TTP, thymidine 5′-triphosphate; CTP, cytidine 5′-triphosphate; IMP, inosine 5′-monophosphate; TMP, thymidine 5′-monophosphate; UMP, uridine 5′-monophosphate; CMP, cytidine 5′-monophosphate; T, thymidine; dC, 2′-deoxycytidine; dA, 2′-deoxyadenosine; dG, 2′-deoxyguanosine; ITU, 7-deaza-7-iodoadenosine; Ap_3A, P^1,P^3-di(adenosine-5′) triphosphate; Ap_4A, P^1,P^4-di(adenosine-5′) tetraphosphate; Ara-A, 9-β-D-arabinofuranosyladenine; NTPs, nucleotide triphosphates; NDPs, nucleotide diphosphates; ORF, open reading frame.

Table 1: Gene-Specific Oligonucleotides Used for the Analysis of *Ag*AK and Its Transcript

template	primers	expected size (bp) with cDNA	expected size (bp) with gDNA
*Ag*PNP (control)	forward, 5′-CACCATGAGCAAATTTAGCTACCTTCAAA-3′ reverse 5′-CTACTTCTTCGCCTCGTAGTGG-3′	1062	2278
*Ag*AK	forward, 5′-GCGCTTCCTTTTTATATAATC-3′ reverse, 5′-TTAATTGTCAGCACAGAAGGACG-3′	1074	1547

revealed a monomeric structure similar to that of *Homo sapiens* adenosine kinase (*Hs*AK), reflecting the 48% identical amino acid sequence.

EXPERIMENTAL PROCEDURES

In Silico A. gambiae Adenosine Kinase Identification. The protein sequence of *H. sapiens* adenosine kinase (*Hs*AK) was used as a query in a tBLASTn search of the *A. gambiae* genome sequence (available in 2003), through the NCBI website (default settings). The *A. gambie* genome was analyzed for the presence of introns, and translations of the exon regions were used for further analyses.

RNA Isolation, cDNA Synthesis, and Polymerase Chain Reaction (PCR) Analysis. Genomic DNA from *A. gambiae* G3 was obtained from MR4. Total RNA was prepared directly from 7−10 frozen adults of *A. gambiae* G3 generation F5 (MRA-132B, MR4) in 2 mL of Trizol (Invitrogen), and RNA was extracted according to the manufacturer's instructions. Subsequent cDNA synthesis was performed with 1 μg of total RNA. The extracted RNA was treated with DNaseI (RNase-free, Invitrogen) before cDNA synthesis, according to the manufacturer's instructions. First-strand cDNA was synthesized by use of Superscript III reverse transcriptase (Invitrogen) and a gene-specific primer mix with 2 pmol of each antisense oligonucleotide or $(dT)_{20}$ as described by the manufacturer. Gene-specific oligonucleotide primers were used for the *Ag*AK gene and for *Ag*PNP [used as a positive control (Table 1)] (*14*). PCRs were performed with Platinum PCR super master mix High Fidelity (Invitrogen) as described by the manufacturer. PCR products from cDNA and gDNA of each gene were sequenced after gel purification.

A. gambiae Adenosine Kinase Gene Construction, Protein Expression, and Purification. A chemically synthesized gene encoding the adenosine kinase from *A. gambiae* was synthesized and cloned into a pDONR221 vector (DNA 2.0). The gene sequence was synthesized using optimized codons for *Escherichia coli* protein expression with an N-terminal thrombin-cleavable hexahistidine tag. The synthetic gene was transferred to the pDEST-14 vector (Invitrogen) with LR-Clonase II (Invitrogen). The pDEST14-*Ag*AK construct was transformed into TOP10 competent cells (Invitrogen) and cultured on LB-carbenicillin agar plates. The plasmid was isolated using a Miniprep Kit (Qiagen) and sequenced using a T7 promotor primer and a T7 terminator primer. The pDEST14-*Ag*AK construct was then introduced into *E. coli* BL21-AI cells (Invitrogen) for expression. The cells were grown in LB-carbenicillin at 37 °C to an OD_{600} of 0.6, induced with L-arabinose at a final concentration of 0.2% (w/v), and grown at 20 °C overnight. Cells were harvested by centrifugation (4000*g* for 30 min) and were ruptured by being passed through a French press. Cell debris was pelleted by centrifugation (16000*g* for 30 min), and the supernatant was purified over a 3 mL Ni-NTA affinity column (Qiagen) with elution by a step gradient of 25, 50, 100, 200, 250, 300, and 500 mM imidazole in 50 mM HEPES (pH 8), 300 mM NaCl, and 1 mM DL-dithiothreitol (DTT). The purified recombinant protein was dialyzed overnight against 50 mM Tris base (pH 7.5) and 1 mM DTT. After dialysis, glycerol was added to a final concentration of 10%, and 50 μL aliquots were frozen in liquid nitrogen and stored at −80 °C. Under these conditions, *Ag*AK retained full activity for several months. Protein concentrations were determined by UV absorbance by use of the extinction coefficient of 27765 M^{-1} cm^{-1} at 280 nm. All enzymatic parameters and crystal structures were obtained with the recombinant *Ag*AK containing the N-terminal hexahistidine tag.

Adenosine Kinase Enzymatic Assays and Inhibition Studies. Adenosine kinase activity was measured using a modified radiometric assay (*15*). Reactions were conducted in 1 mL at 27 °C in 50 mM Tris buffer (pH 7.4) containing 5 mM $MgCl_2$, 50 mM KCl, 0.2 mM DTT, and varying concentrations of ATP and [2-^{3}H]adenosine (23 Ci/mmol, Amersham Biosciences) as appropriate. Reactions were initiated by the addition of enzyme and terminated by spotting 40 μL onto DE81 filters (Whatman). Aliquots were taken at 1 min intervals over the course of a 5 min assay. Dried filters were washed three times with 5 mL of water and once with 5 mL of 95% ethanol and dried at room temperature. Filters were subjected to liquid scintillation counting in 10 mL of Betaplate Scint (PerkinElmer). An enzyme-free control for each concentration was used to subtract background. The apparent K_m value for adenosine was determined at 1 mM ATP and 5 mM $MgCl_2$ using [2-^{3}H]adenosine concentrations ranging from 1 to 75 nM and 0.1 nM *Ag*AK. The apparent K_m value for ATP was obtained at 0.5 μM [2-^{3}H]adenosine with ATP concentrations ranging from 0.1 to 50 μM, 5 mM $MgCl_2$, and 5 nM *Ag*AK. Kinetic parameters were calculated from Michaelis−Menten analysis of initial rate data.

Enzyme inhibition assays to determine K_i values were performed using different concentrations of iodotubercidin (ITU, 7-deaza-7-iodoadenosine, Berry and Associates), P^1,P^3-di(adenosine-5′) triphosphate ammonium salt (Ap_3A, Sigma) or P^1,P^4-di(adenosine-5′) tetraphosphate ammonium salt (Ap_4A, Sigma), 50 nM [2-^{3}H]adenosine, 1 mM ATP, and 5 mM $MgCl_2$. The inhibition constants were determined as described previously (*16*) with inhibitor concentrations ranging from 1 to 100 nM. Reaction mixtures with different ITU concentrations were filtered through a YM10 Centricon spin column [molecular weight (MW) retention of 10000 (Amicon)] and analyzed by high-performance liquid chromatography to test for substrate activity with *Ag*AK.

Analysis of Enzymatic Reactions by High-Performance Liquid Chromatography (HPLC). Samples were analyzed with a reverse-phase [Luna C_{18}(2), 150 mm × 4.6 mm, 5 μm, Phenomenex] ion pair HPLC system. The mobile phases were 8 mM tetrabutylammonium bisulfate (Fluka) and 100 mM KH_2PO_4 with the pH adjusted to 6.0 with KOH (solution A) and 30% acetonitrile containing 8 mM tetrabutylammonium bisulfate and 100 mM KH_2PO_4 (pH 6) as solution B. The HPLC

gradient was from 0 to 100% solution B over 20 min. The eluant was monitored at 254 nm, and the flow rate was 1 mL/min.

Adenosine Kinase Substrate Specificity Assays. *Ag*AK nucleoside specificity was measured using the method described above. Reactions were conducted in 100 μL at 27 °C in 50 mM Tris buffer (pH 7.4) containing 5 mM $MgCl_2$, 50 mM KCl, 0.2 mM DTT, 1 mM ATP, and 0.5 μM [2-^{3}H]adenosine, [8-^{3}H]guanosine (15 Ci/mmol, American Radiolabeled Chemicals Inc.), [5-^{3}H]cytidine (25 Ci/mmol, Sigma), [5-^{3}H]uridine (27.2 Ci/mmol, Perkin-Elmer), [8-^{3}H]inosine (27 Ci/mmol, American Radiolabeled Chemicals Inc.), [8-^{14}C]-2′-deoxyadenosine (48.8 mCi/mmol, Sigma), [8-^{14}C]-2′-deoxyguanosine (55 mCi/mmol, Sigma), [5-^{3}H]-2′-deoxycytidine (20 Ci/mmol, American Radiolabeled Chemicals Inc.), [5-^{3}H]thymidine (12.9 Ci/mmol, Amersham Biosciences), or [1-^{3}H]ribose (15 Ci/mmol, Sigma). For inhibitor or subversive substrate screening, reactions were performed with 0.5 μM [2-^{3}H]adenosine, 1 mM ATP, and 75 μM 9-β-D-arabinofuranosyladenine (Ara-A, Sigma) or ITU. In all cases, reactions were initiated by the addition of enzyme and terminated after incubation for 10 min by spotting 40 μL onto DE81 filters (Whatman). A blank (no enzyme) for each radiolabeled substrate was used to subtract unmetabolized radiolabeled substrate bound to DE81 filters. The specific activity is expressed relative to activity with adenosine.

Adenosine kinase activity as a function of GTP, UTP, CTP, and TTP concentrations was measured using a luminescence assay (*17*). In this assay, AMP generated from adenosine and NTPs by reaction with *Ag*AK is converted to ATP by pyruvate orthophosphate dikinase (PPDK). ATP and luciferin are converted to light and AMP by firefly luciferase. The AMP formed in the luciferase reaction is cycled via PPDK to give a sustained luminescence signal. K_m values for adenosine were determined with fixed NTP concentrations of 100 μM, adenosine concentrations from 0.2 to 2 μM, and 4 nM *Ag*AK. In a similar way, the K_m values for the NTPs were measured with a fixed concentration of 10 μM adenosine, NTP concentrations varying from 30 to 200 μM, and 4 nM *Ag*AK. Kinetic parameters (k_{cat}, K_m, and catalytic efficiencies) were determined from fits to the Michaelis−Menten equation.

Crystallization, Data Collection, and Structural Determination. *Ag*AK was concentrated to 11.7 mg/mL and incubated on ice with 1 mM Ap_4A and 5 mM $MgCl_2$ in 50 mM HEPES buffer (pH 7.5), containing 500 mM NaCl. The enzyme was crystallized in 25% PEG3350, 0.2 M $MgCl_2$, 5% 2-propanol, 25% glycerol, and 0.1 M BisTris buffer (pH 5.5) using the sitting drop vapor diffusion method at 18 °C. Crystals were freshly frozen in liquid N_2 before data were collected.

X-ray diffraction data of Ap_4A-bound *Ag*AK were collected at beamline X29A of the Brookhaven National Laboratory on an ADSC Q315 detector at 100 K. Data were processed with the HKL2000 program suite, and data processing statistics are listed in Table 2 (*18*).

The crystal structure of *Ag*AK was determined by molecular replacement in Molrep using the published structure of human adenosine kinase (Protein Data Bank entry 1BX4) as the search model (*19*). The initial atomic model was rebuilt with PHENIX (*20*). The model without ligand was first rebuilt in COOT and refined in Refmac5 (*21*, *22*). The ligands were later added in COOT using the $F_o - F_c$ map when R_{free} is below 30% and refined in Refmac5. A chloride ion near the adenine binding site was added on the basis of the crystallization condition and the presence of a chloride ion at a similar position in the human AK structure (Protein Data Bank entry 1BX4). Two of three catalytic Arg131 side chain residues where the electron density is weak were built by pointing the side chain away from bound Ap_4A. The final model was validated with Procheck (*23*). Refinement statistics are summarized in Table 2. The coordinates and structure factors for Ap_4A-bound *Ag*AK were deposited in the Protein Data Bank as entry 3LOO.

Table 2: Data Collection and Refinement Statistics[a] of Ap_4A-Bound *Ag*AK (Protein Data Bank entry 3LOO)

Data Collection	
space group	$P2_1$
cell dimensions	
a, *b*, *c* (Å)	50.4, 76.8, 140.5
α, *β*, *γ* (deg)	90.0, 92.1, 90.0
resolution (Å)	20.00−2.00 (2.07−2.00)[b]
R_{sym} (%)	6.8 (54.7)[b]
$I/\sigma I$	19.5 (2.1)[b]
completeness (%)	100.0 (99.8)[b]
redundancy	3.7 (3.6)[b]
Refinement	
resolution (Å)	20.00−2.0
no. of reflections	72380
R_{work}/R_{free} (%)	19.8/24.7
B factor (Å^2)	
protein	
main chain	38.8
side chain	41.0
water	39.9
ligand	37.4
no. of atoms	
protein	7753
water	242
ligand	165
root-mean-square deviation	
bond lengths (Å)	0.014
bond angles (deg)	1.50
Ramanchran analysis (%)	
allowed region	99.3
disallowed region	0.7
coordinate error by Luzzati plot (Å)	0.25

[a]One crystal was used for each data set. [b]Numbers in parentheses are for the highest-resolution shell.

RESULTS

Identification and Expression of Recombinant A. gambiae Adenosine Kinase. The presence of adenosine kinase in the *A. gambiae* genome was suggested previously but not established (*14*). The *A. gambiae* AK was located from its similarity to the amino acid sequence of *H. sapiens* AK (GenBank entry CAI39671.1) by BLAST analysis. A genomic region whose proposed translation showed a high level of similarity to the *H. sapiens* enzyme was retrieved (Figure 1). Conceptual translation of this region resulted in a 348-amino acid protein, representing a putative *A. gambiae* AK. The presence of this gene and its transcript in *A. gambiae* was confirmed by PCR amplification of *A. gambiae* gDNA and cDNA (Figure 2). RT-PCR analysis of the mosquito total RNA and mRNA revealed that *Ag*AK is transcribed in adult mosquitoes.

Kinetic Parameters, Substrate Specificity, and Inhibition of AgAK. *Ag*AK activity was measured by the production of [^{3}H]AMP from [^{3}H]adenosine. Steady-state kinetics for *Ag*AK indicated a K_m value of 8.1 ± 0.6 nM for adenosine and a K_m of

```
                  *        20         *        40         *        60
A.gambiae : -----------------MESLRDGMLVGLGNPLLDISAVVEKDLLNKYDMQPNNAILAEEKHMPM :  48
H.sapiens : MAAAEEEPKPKKLKVEAPQALRENILFGMGNPLLDISAVVDKDFLDKYSLKPNDQILAEDKHKEL :  65
T.gondii  : -----------MAVDSSNSATGPMRVFAIGNPILDLVAEVPSSFLDEFFLKRGDATLATPEQMRI :  54

              *        80         *       100         *       120         *
A.gambiae : YQELIEKYQAEYIAGGSVQNSLRVAQWILQRP-RTAIFFGCVGQDEYARILEERATSNGVNVQYQ : 112
H.sapiens : FDELVKKFKVEYHAGGSTQNSIKVAQWMIQQPHKAATFFGCIGIDKFGEILKRKAAEAHVDAHYY : 130
T.gondii  : YST-LDQFNPTSLPGGSAINSVRVVQKLLRKP-GSAGYMGAIGDDPRGQVLKELCDKEGLATRFM : 117

                  140         *       160         *       180         *
A.gambiae : RSATSPTGTCAVLVTGTQRSLCANLAAANDFTP-EHLRSDGNRAYLQGAQFFYVSGFFFTVSFES : 176
H.sapiens : EQNEQPTGTCAACITGDNRSLIANLAAANCYKKEKHLDLEKNWMLVEKARVCYIAGFFLTVSPES : 195
T.gondii  : VAPGQSTGVCAVLINEKERTLCTHLGACGSFRLPEDWTT-----FASGALIFYATAYTLTATPKN : 177

                200         *       220         *       240         *       260
A.gambiae : AISVAKEAA-ATGRMFMMNLSAPFVPQFYKNNLEEIFPYVDVLFGNETEAIALAKEFNYGTEDLR : 240
H.sapiens : VLKVAHHAS-ENNRIFTLNLSAPFISQFYKESLMKVMPYVDILFGNETEAATFAREQGFETKDIK : 259
T.gondii  : ALEVAGYAHGIPNAIFTLNLSAPFCVELYKDAMQSLLLHTNILFGNEEEFAHLAKVHNLVAAEKT : 242

                  *       280         *       300         *       320
A.gambiae : EIGKR-------------IAALPKENGKRKRIVIITQGSDPVLLIEAGTD---NVREFPVQKLAP : 289
H.sapiens : EIAKK-------------TQALPKMNSKRQRIVIFTQGRDDTIMATES-----EVTAFAVLDQDQ : 306
T.gondii  : ALSTANKEHAVEVCTGALRLLTAGQNTGATKLVVMTRGHNPVIAAEQTADGTVVVHEVGVPVVAA : 307

                *       340         *       360         *       380
A.gambiae : EQMVDTNGAGDAFVGGFLAQLLQSRTVDVCIKCGIWAAREIIQRSGCTFEGEPSFCADN : 348
H.sapiens : KEIIDTNGAGDAFVGGFISQIVSDKPLTECIRAGHYAASIIIRRTGCTFPEKPDFH--- : 362
T.gondii  : EKIVDTNGAGDAFVGGFIYAISQGKTVKQCIMCGNACAQDVIQHVGFSLSFTSLPC--- : 363
```

FIGURE 1: Multiple-sequence alignment of the predicted amino acid sequence of *A. gambiae* with the known adenosine kinases from human (*H. sapiens*) and *Toxoplasma gondii*. The amino acid sequence of *Hs*AK was used to search the *A. gambiae* genome by BLAST analysis. The *Ag*AK sequence is 48% identical and 19% similar to the *Hs*AK sequence while only 31% identical and 20% similar to the *Tg*AK sequence.

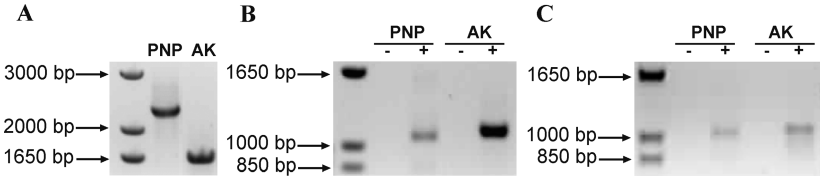

FIGURE 2: Presence of adenosine kinase gene and its transcript in *A. gambiae* confirmed by PCR of *A. gambiae* gDNA and cDNA in adult mosquitoes. (A) gDNA analysis revealed the expected size for the adenosine kinase predicted gene. (B) PCR performed using cDNA generated by RT-PCR using gene-specific oligonucleotide primers (total RNA). (C) PCR performed using cDNA generated by RT-PCR using oligo(dT)$_{20}$ primers (mRNA).

1.4 ± 0.4 μM for ATP (Table 3). The turnover number of the enzyme was calculated to be 0.16 s^{-1} at a saturating ATP concentration and 0.3 s^{-1} at a saturating adenosine concentration. The k_{cat}/K_m values with respect to ATP and adenosine are 2.4×10^5 and 1.97×10^7 M^{-1} s^{-1}, respectively, and are near the diffusion limit for enzymatic catalysis. With these K_m values, the enzyme *in vivo* is saturated with respect to ATP and is designed to capture adenosine and phosphorylate with high efficiency. The low k_{cat} is a kinetic requirement because of the unusually tight binding by adenosine. Similar to other adenosine kinases, the *Ag*AK enzyme is inhibited at high concentrations of adenosine. Thus, experimental k_{cat} values depend on the fixed adenosine concentrations. To determine the K_m for ATP, a higher concentration of enzyme was used. The *Ag*AK enzyme exhibits narrow nucleoside specificity with weak deoxyribonucleoside kinase activity (Figure 3A). The 9-β-D-arabinofuranosyladenine (Ara-A) analogue of adenosine at concentrations in 150-fold excess over adenosine did not affect the *Ag*AK activity (Figure 3B), while iodoturbecidin (ITU) inhibited with an apparent K_i of 1 nM (Table 3). Recognition of ITU as a substrate by *Ag*AK was also assayed by HPLC analysis because the radiochemical assay does not distinguish conventional inhibition from competition as a substrate. No phosphorylation was detected indicating that ITU acts as an inhibitor of the enzymatic activity and not as a subversive substrate. Inhibition assays to determine the K_i values for ITU, Ap_3A, and Ap_4A used 50 nM [2-^{3}H]adenosine and 1 mM ATP (Table 3). Ap_4A and Ap_3A are well-known bisubstrate analogues of adenosine kinases, and surprisingly, these bind with relatively weak affinities of 0.86 and 61 μM, respectively (Table 3).

*Ag*AK is highly specific for adenosine as the nucleoside substrate, but the substrate specificity for the phosphoryl donor is broader. The enzyme utilizes the γ-phosphoryl from ATP, GTP, UTP, CTP, or TTP (Table 3) and with all phosphoryl donors *Ag*AK is relatively efficient in converting adenosine to AMP (k_{cat}/K_m values with respect to adenosine from 2.7×10^6 to 1.97×10^7 M^{-1} s^{-1}). The k_{cat}/K_m values with respect to NTPs are lower (from 1.09×10^3 to 2.4×10^5 M^{-1} s^{-1}) because of weaker binding of the

Table 3: Kinetic Parameters and Inhibition Constants of *Ag*AK

	Adenosine[a]		
	K_m (nM)	k_{cat} (s^{-1})	k_{cat}/K_m (M^{-1} s^{-1})
ATP	8.1 ± 0.6	0.160 ± 0.003	(1.97 ± 0.04) × 10^7
GTP	230 ± 10	0.63 ± 0.01	(2.7 ± 0.1) × 10^6
UTP	740 ± 50	0.035 ± 0.002	(4.7 ± 0.4) × 10^6
CTP	630 ± 50	0.029 ± 0.001	(4.6 ± 0.4) × 10^6
TTP	790 ± 80	0.056 ± 0.004	(7.1 ± 0.9) × 10^6
	NTP[b]		
	K_m (μM)	k_{cat} (s^{-1})	k_{cat}/K_m (M^{-1} s^{-1})
ATP	1.4 ± 0.4	0.33 ± 0.02	(2.4 ± 0.5) × 10^5
GTP	54 ± 5	1.39 ± 0.07	(2.6 ± 0.3) × 10^4
UTP	56 ± 2	0.061 ± 0.001	(1.09 ± 0.04) × 10^3
CTP	49 ± 3	0.062 ± 0.002	(1.27 ± 0.09) × 10^3
TTP	245 ± 74	0.30 ± 0.07	(1.2 ± 0.5) × 10^3
			K_i (nM)
ITU			1.0 ± 0.2
Ap_4A			860 ± 130
Ap_3A			61000 ± 13000

[a] K_m values for adenosine were determined at fixed concentrations of 100 μM of each NTP with other conditions as described in Experimental Procedures. [b] K_m values for the NTPs were determined at fixed concentrations of 10 μM adenosine with other conditions as described in Experimental Procedures.

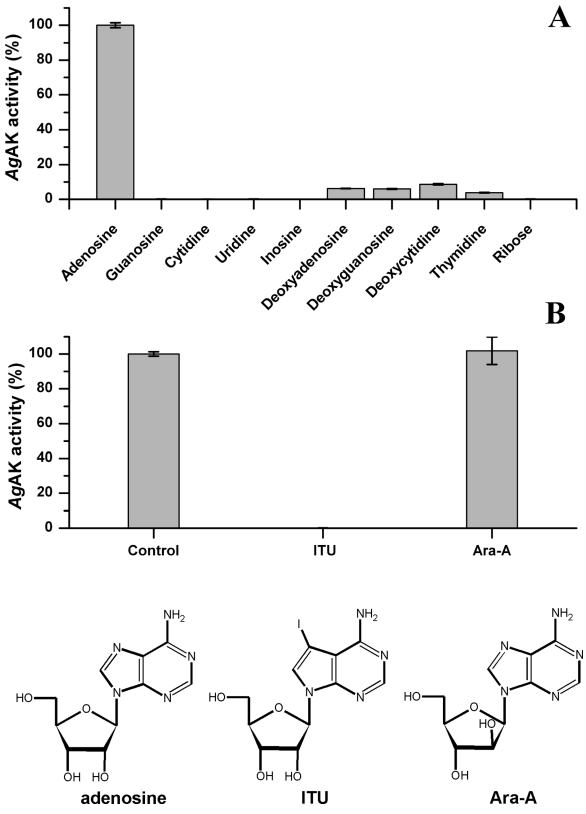

FIGURE 3: Substrate specificity for *Ag*AK. (A) The nucleoside specific activities are relative to the activity with adenosine (shown to give a k_{cat} of 0.16 s^{-1} and a k_{cat}/K_m of 2.0 × 10^7) that was set to 100% for each fraction. *Ag*AK exhibited partial deoxyribonucleoside kinase activity. (B) Adenosine analogue Ara-A and ITU tested as potential inhibitor and/or subversive substrate of *Ag*AK at concentrations in 150-fold excess over that of adenosine. Activity was relative to the activity of control were only adenosine and ATP were present in the reaction mixture.

phosphoryl donors. Purine triphosphates ATP and GTP have better efficiencies (2.4 × 10^5 and 2.6 × 10^4 M^{-1} s^{-1}, respectively), while pyrimidine triphosphates UTP, CTP, and TTP have lower efficiencies (from 1.09 × 10^3 to 1.27 × 10^3 M^{-1} s^{-1}).

Overall Structure and Inhibitor Binding. The crystal structure of *Ag*AK was determined to 2.0 Å resolution. The enzyme is a monomer with three *Ag*AK molecules in the asymmetric unit. All contained Ap_4A and Mg^{2+} in the active sites. *Ag*AK consists of two domains (Figure 4). The small domain located at the N-terminus is responsible for adenosine interactions and consists of the secondary structure elements helix α1, helix α2, and β-strands β2−β4, β7, and β8. The large ATP-binding domain has a typical α/β structure as well as conserved kinase anion hole motifs where the phosphates of ATP bind (*24*). The overall structure of the three *Ag*AK molecules in the asymmetric unit is almost identical (the root-mean-square deviations of the Cα backbone of residues 10−333 are 0.2−0.3 Å). However, subtle differences are seen in the region near the catalytic site Arg131. In two *Ag*AK molecules, the electron density of the side chain of Arg131 is well-defined while the region from residue 288 to 295 is disordered (Figure 5A,B). In the third *Ag*AK molecule, the electron density of the side chain of Arg131 is weak, but residues 288−295 are ordered with well-defined electron density (Figure 5C). We interpret these differences to represent catalytic site motions linked to formation of a catalytically competent complex (see Discussion).

*Ag*AK accommodates the tripolyphosphate from ATP in the catalytic site prior to phosphoryl transfer. However, the Ap_4A bound to *Ag*AK has a tetraphosphate and is a better mimic of ATP and AMP than the normal reactants (ATP with adenosine or ADP with AMP). Polyphosphate chains are flexible, and instead of pushing aside the adenosine moieties, the four phosphoryl groups fit tightly into the tripolyphosphate binding site in a geometry to resemble phosphoryl transfer. The oxygen equivalent to the 5′-hydroxyl of adenosine (the nucleophilic oxygen) is 2.9 Å from the γ-phosphorus of the ATP mimic. By comparison, the nucleophilic adenosine oxygen is located 4 Å from the β-phosphorus of the ATP moiety (Figure 6). A magnesium ion is positioned between the β- and γ-phosphoryl groups to form an octahedral (hexacoordinate) complex with two oxygen atoms from the β- and γ-phosphoryl of the ATP moiety and four coordinated water molecules (Figure 7). Three of the coordinated water molecules form hydrogen bonds with neighboring residues, including side chains of Asn194, Ser196, Glu224, and Asp300. The γ-phosphoryl of the ATP moiety accepts hydrogen bonds from the amides of Gly299 and Asp300. The α-phosphoryl of the ATP moiety forms hydrogen bonds to the side chains of Thr263 and the amide of Gly265. The phosphoryl from AMP makes a hydrogen bond to the amide of Gly297 (Figure 7). The adenine of ATP is partially buried in a hydrophobic pocket formed by Val269, Leu287, Ile324, Ala327, and Ile331. N1 of ATP forms a hydrogen bond to the amide of Leu287, and O3′ interacts with a hydrogen bond to the amide of Gln264 via a water molecule. The adenosine from the AMP moiety forms an anticlinal conformation, and the ribose of AMP has an O4′-endo sugar pucker conformation. The adenine of the AMP moiety is surrounded by hydrophobic residues, including Leu16, Leu40, Leu133, Ala135, Leu137, and Phe168. In the *Ag*AK molecule where residues 288−294 are ordered, Met292 is

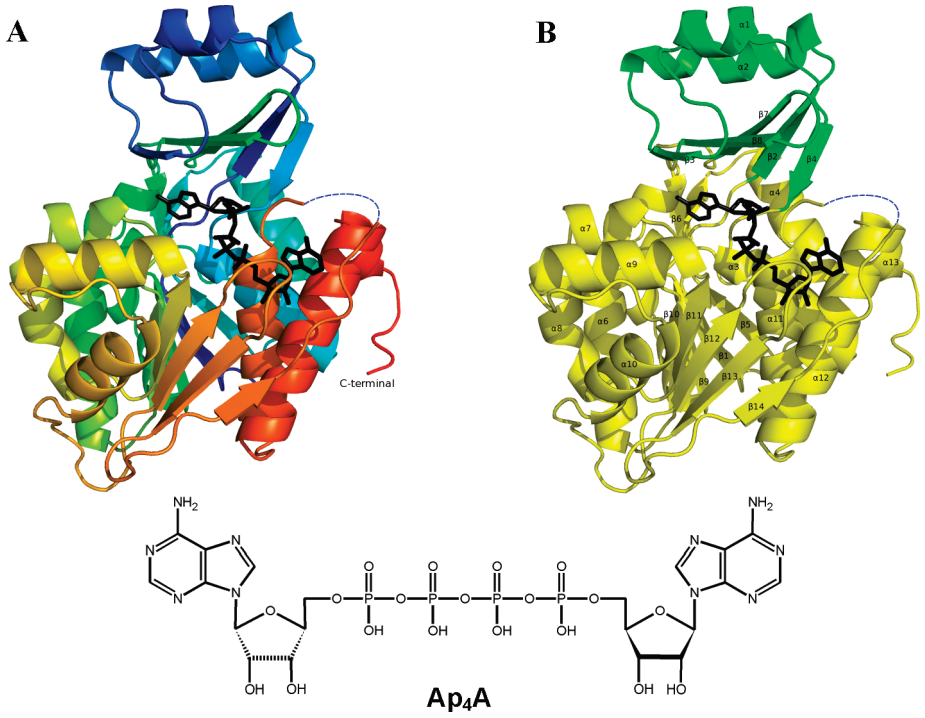

FIGURE 4: Ap_4A-bound *Ag*AK structure depicted as a ribbon diagram. (A) The Ap_4A-bound *Ag*AK is colored from blue (N-terminus) to red (C-terminus), and Ap_4A is depicted as black sticks. The disordered region (residues 289−294) is represented as a blue dashed line. (B) The small domain (residues 17−62 and 121−136) of *Ag*AK and the large domain (the remaining residues) of *Ag*AK are colored green and yellow, respectively. The disordered region (residues 289−294) is represented as a blue dashed line.

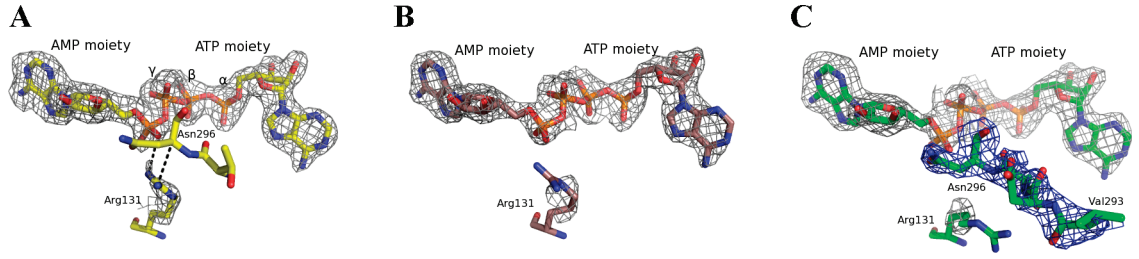

FIGURE 5: Interactions of Ap_4A with the side chain of Arg131 and corresponding $F_o - F_c$ omit electron density (gray) contoured at 2.5σ. Strong electron density is observed for Ap_4A bound to the three *Ag*AK molecules in the asymmetric unit. (A) First *Ag*AK molecule where electron density is clearly shown at the side chain of Arg131. The side chain of Arg131 hydrogen bonds to the phosphate from the AMP moiety and is in the proximity of the backbone of Asn296. Distances shorter than 3.2 Å are represented as black dashed lines. (B) Second *Ag*AK molecule, for which the electron density of the guanidine group of Arg131 is missing. (C) Third *Ag*AK molecule, for which the electron density of the side chain of Arg131 is almost absent but strong density of the backbone of residues 288−295 is observed. The $2F_o - F_c$ electron density map (at 1σ) from Val293 to Asn296 is colored blue.

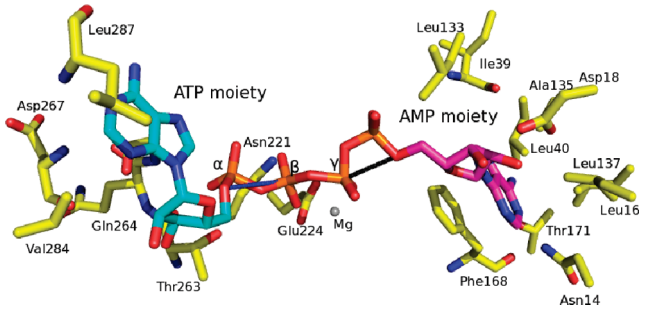

FIGURE 6: Conformation of Ap_4A in the actives sites. The adenine from the ATP moiety and the adenine from the AMP moiety are colored cyan and purple, respectively. The α-, β-, and γ-phosphate molecules from the ATP moiety are labeled. The distance of 2.9 Å between the 5′-hydroxyl of AMP and the γ-phosphate of ATP is represented as a black line. The distance of 4.0 Å between the 5′-hydroxyl of ATP and the β-phosphate of ATP is represented as a blue line. A subset of the active site residues are depicted as sticks.

near the adenine. N1 of AMP accepts a hydrogen bond from the side chain of Asn14, and a water molecule mediates the hydrogen bonding between N9 of AMP and the amide of Ile39. Water molecules also mediate the hydrogen bonding among the N6 amino group of AMP, the side chain of Thr171, and the carbonyl of Phe168. O2′ and O3′ of AMP both make hydrogen bonds to the side chain of Asp18. In addition, O2′ and O3′ from the AMP moiety make hydrogen bonds to the amide of Gly64 and the side chain of Asn68, respectively. A chloride molecule, which is also present in the crystal structures of the liganded human and *T. gondii* AKs, is found 3.5 Å from C2 of the AMP moiety. The function of this chloride is not apparent from the structure and may be charge neutralization. The rmsd of the Cα backbone in reference to liganded *Hs*AK and *Tg*AK is between 1 and 1.5 Å.

DISCUSSION

Identification and Characterization of Adenosine Kinase from A. gambiae. Mosquitoes grown in semisynthetic media

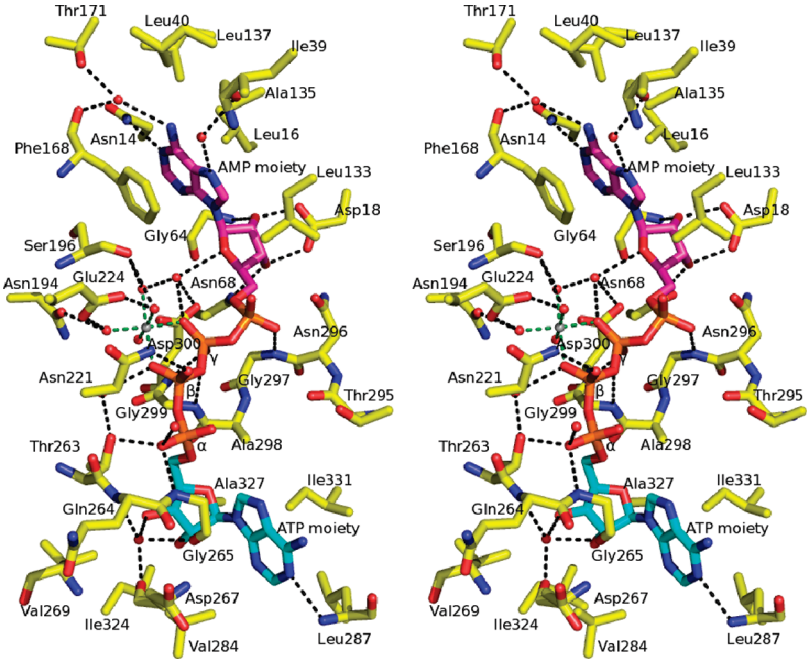

FIGURE 7: Stereoview of Ap_4A bound to *Ag*AK and its surrounding residues. The adenine from the ATP moiety and the adenine from the AMP moiety are colored cyan and purple, respectively. The magnesium and water molecules are depicted as gray and red dots, respectively. The α-, β-, and γ-phosphate molecules from the ATP moiety are labeled. The magnesium−oxygen and hydrogen bonds are represented as green and black dashed lines, respectively.

revealed dietary requirements for AMP (or IMP), TMP, and UMP (or CMP) or the corresponding nucleosides (*25*). The requirement for these metabolites suggested that purine and pyrimidine salvage pathways may be important in *Anopheles* nucleotide metabolism. Adenosine kinase has a key role in adenosine salvage in maintaining the ATP pool, particularly in cells with no *de novo* purine synthesis, including human erythrocytes. Ribonucleoside and deoxyribonucleoside kinases serve to trap nucleosides within cells by phosphorylation and may be involved both in the maintenance of the ATP pool and in the buildup of other nucleic acid precursors. Here, the full-length ORF of *Ag*AK (Figure 1) was overexpressed as a fusion protein with a His tag. The presence of an AK gene and its transcript in *A. gambiae* adult mosquitoes was confirmed by PCR of *A. gambiae* genomic DNA and its cDNA (Figure 2). The kinetic parameters for the recombinant protein revealed the lowest K_m reported for any adenosine kinase (Table 3). The low K_m, high k_{cat}/K_m, and substrate inhibition observed for the recombinant *Ag*AK suggest that this enzyme provides an efficient salvage mechanism in the adenosine metabolism of *A. gambiae*. In humans, AK is the most important enzyme for maintenance of the ATP pool in erythrocytes. Although its kinetic properties suggest an important role in adenosine salvage, further metabolic studies are needed to reveal the biological function of this enzyme in mosquitoes.

*Ag*AK has narrow nucleoside specificity, supporting a specific role in adenosine salvage (Figure 3A). Previous work suggested three proteins with deoxyribonucleoside kinase activity in cell extracts from *A. gambiae* cell culture on DEAE-ion exchange chromatography. The major peak was a multisubstrate deoxyribonucleoside kinase (*Ag*dNK), and the other peaks had adenosine kinase activity with partial deoxyribonucleoside kinase activity (*26*). One of these exhibited substrate specificity consistent with the *Ag*AK described here, supporting expression of this activity *in vivo* (*26*). The nucleoside specificity of adenosine kinases characterized from other organisms is usually broader than their nucleotide triphosphate specificity (*7*, *10*, *15*, *27*, *28*). For example, the AK from *T. gondii* uses ITU and other 6-substituted analogues as nucleoside substrates (*8*, *24*), whereas *Ag*AK cannot. The *Ag*AK enzyme is unusual in its high specificity for adenosine with lower activity on deoxyribonucleosides (Figure 3A,B). The enzyme has a broad NTP specificity using ATP, GTP, UTP, TTP, and CTP as phosphoryl donors (Table 3).

Inhibition of *Ag*AK by ITU showed a K_i value of 1 nM, a surprisingly powerful inhibitor considering the narrow nucleoside specificity of this enzyme (Table 3). However, the unusually tight interaction with adenosine (K_m = 8.1 nM) gives a modest K_m/K_i of 8.1. Ap_4A and Ap_3A are well-known bisubstrate analogues of adenosine kinases, and surprisingly, these bind with relative weak affinities of 0.86 and 61 μM, respectively (Table 3).

AgAK Crystal Structure. The overall topology of *Ag*AK showed a high degree of similarity to the human (*Hs*AK) and *T. gondii* AK (*Tg*AK) topologies. Like the human and *T. gondii* AK structures, the *Ag*AK structure contains a mixed fold and consists of small and large domains (Figure 4). The fold belongs to the ribokinase-like family with a small and large Rossmann fold domain. The large domain, termed the catalytic core, is a three-layer α/β/α sandwich, and the small domain, termed the cap, is in contact with the substrate, adenosine. In *Tg*AK, the cap domain rotates 30° upon adenosine or ITU binding, inducing a fully closed conformation (*24*), but this rotation is not observed when ATP analogues are bound (*29*). Furthermore, a semiclosed or semiopened conformation in which the small lid region undergoes a rigid-body rotation of ~12° was observed in *Tg*AK bound to adenosine analogues N^6,N^6-dimethyladenosine (DMA) and 6-methylmercaptopurine riboside (MMPR) (*30*). Despite our efforts, the *Ag*AK failed to crystallize in the apo form or with ITU, and the cocrystallization with Ap_4A succeeded only after an extensive screening to give a crystal structure similar to the closed conformation.

The catalytic site of *Ag*AK normally accommodates three phosphoryl groups together with the 5′-hydroxyl group as the incipient nucleophile. However, the Ap_4A bound to *Ag*AK consists of four phosphoryl groups that fit tightly into the phosphate binding site, keeping the adenosine and ATP binding groups in place. Interestingly, Ap_4A (K_i = 860 nM) exhibited tighter binding than Ap_3A (K_i = 61000 nM) (Table 3). Ap_3A is one atom short of the productive catalytic site complex, and a similar binding pattern has been found for Ap_5A with adenylate kinase, where the extra phosphoryl group is required to allow alignment of groups in the catalytic site to mimic the geometry similar to a trigonal bipyramid needed for terminal phosphoryl transfer (*31*).

The *Ag*AK active site residues that involve hydrogen bonding and hydrophobic interaction with adenosine are either conserved or replaced with similar amino acids when compared to *Hs*AK and *Tg*AK (Figure 1). From the structural point of view, there is no clear evidence to illustrate why *Ag*AK can capture adenosine more efficiently than *Hs*AK and *Tg*AK. However, the relatively high K_m value of *Tg*AK for adenosine may due to the replacement of Phe168 with Tyr that involves hydrophobic stacking with adenosine. Substrate on and off rates from catalytic sites dictate the affinity; thus, dynamic components not readily apparent from the crystal structure are likely to be involved. The levels of sequence identity of *Hs*AK and *Tg*AK relative to *Ag*AK are 48 and 31%, respectively. Thus, catalytic site efficiency of *Ag*AK may also be contributed by residues remote from the adenosine binding site. As an example, the 30° rotation of the cap domain required for adenosine binding in *Tg*AK (*24*) may differ in *Ag*AK because amino acid residues in the hinge region differ and may change the dynamics of the rotation motion and therefore the on−off frequency and binding affinity. The structural comparison showed Tyr60, Tyr94, and Asn136 in *Ag*AK are replaced with Ser, Arg, and His, respectively, in the *Tg*AK structure. Furthermore, Tyr49 in *Ag*AK, which forms a hydrogen bond to the carbonyl of Cys134, is replaced with a Phe in *Hs*AK.

Tight Binding of ITU. Factors contributing to the binding (1.6 μM) of ITU to *Tg*AK include the displacement of an ordered water molecule near N7 of adenosine being replaced with the relatively large and hydrophobic iodine atom (*24*). As this region in *Tg*AK is hydrophobic, surrounded by Ala44, Leu46 (adenosine domain), Cys127, Leu138, Thr140, Tyr169, and Phe201 (ATP domain), more favorable interactions are made. These residues are completely conserved in *Ag*AK except for the conservative Thr140Ala and Tyr169Phe replacements found in *Ag*AK. Although *Ag*AK did not crystallize with ITU, the level of sequence similarity and high affinity of ITU (1 nM) support an even more favorable interaction with the catalytic site residues in *Ag*AK.

Catalytic Arginine. It has been proposed that the closure of the small domain of AK brings the conserved catalytic arginine to the active site when adenine is bound (*24*). The catalytic arginine forms a hydrogen bond to the γ-phosphate of ATP and orients the γ-phosphate into the catalytic position for the S_N2 reaction (*24*). In the crystal structure of Ap_4A bound to *Ag*AK, the small domains of all three *Ag*AK molecules in the asymmetric unit are in the closed conformation. However, the side chains of the catalytic Arg131 either interact with the phosphate from the AMP moiety or move freely (Figure 5). The side chain of the catalytic Arg131 is closer to the phosphate from AMP than to the γ-phosphate of ATP. The arginine is near the backbone of Asn296 when the catalytic Arg131 interacts with the phosphate from the AMP moiety (Figure 5A). Thus, residues near Asn296 are disordered when the side chain of Arg131 forms a hydrogen bond to Ap_4A. This motion may be linked to the phosphoryl transfer in the normal reaction.

Conclusions. Properties of adenosine kinase from the mosquito suggest an important role in adenylate nucleotide pool regulation. The ability to salvage adenosine by a kinase separates the insect host from the parasite and provides a rationale for metabolic and inhibitor design studies for investigating targets in host−parasite interactions. Because malaria infections involve only a few parasites transmitted from human host to human recipient, the insect vector represents a biological bottleneck where interruption of metabolism of only a few parasites can break the infective cycle. Characterization of *Ag*AK adenosine kinase provides biochemical access to this unusual step in host−parasite metabolism.

ACKNOWLEDGMENT

We thank MR4 for providing us with *A. gambiae* mosquitoes contributed by Mark Q. Benedict and William E. Collins and genomic DNA from *A. gambiae* contributed by William E. Collins. Data of X-ray diffraction for this study were recorded at beamline X29A of the National Synchrotron Light Source. Financial support of beamline X29A of the National Synchrotron Light Source comes principally from the Offices of Biological and Environmental Research and of Basic Energy Sciences of the U.S. Department of Energy and from the National Center for Research Resources of the National Institutes of Health.

REFERENCES

1. Snow, R. W., Guerra, C. A., Noor, A. M., Myint, H. Y., and Hay, S. I. (2005) The global distribution of clinical episodes of *Plasmodium falciparum* malaria. *Nature 434*, 214–217.
2. de Koning, H. P., Bridges, D. J., and Burchmore, R. J. S. (2005) Purine and pyrimidine transport in pathogenic protozoa: From biology to therapy. *FEMS Microbiol. Rev. 29*, 987–1020.
3. Hyde, J. E. (2007) Targeting purine and pyrimidine metabolism in human apicomplexan parasites. *Curr. Drug Targets 8*, 31–47.
4. Cassera, M. B., Hazleton, K. Z., Riegelhaupt, P. M., Merino, E. F., Luo, M., Akabas, M. H., and Schramm, V. L. (2008) Erythrocytic adenosine monophosphate as an alternative purine source in *Plasmodium falciparum*. *J. Biol. Chem. 283*, 32889–32899.
5. Spychala, J., Datta, N. S., Takabayashi, K., Datta, M., Fox, I. H., Gribbin, T., and Mitchell, B. S. (1996) Cloning of human adenosine kinase cDNA: Sequence similarity to microbial ribokinases and fructokinases. *Proc. Natl. Acad. Sci. U.S.A. 93*, 1232–1237.
6. Boison, D. (2006) Adenosine kinase, epilepsy and stroke: Mechanisms and therapies. *Trends Pharmacol. Sci. 27*, 652–658.
7. Galazka, J., Striepen, B., and Ullman, B. (2006) Adenosine kinase from *Cryptosporidium parvum*. *Mol. Biochem. Parasitol. 149*, 223–230.
8. Kim, Y. A., Rawal, R. K., Yoo, J., Sharon, A., Jha, A. K., Chu, C. K., Rais, R. H., Al Safarjalani, O. N., Naguib, F. N., and El Kouni, M. H. (2010) Structure-activity relationships of carbocyclic 6-benzylthioinosine analogues as subversive substrates of *Toxoplasma gondii* adenosine kinase. *Bioorg. Med. Chem. 18*, 3403–3412.
9. Ugarkar, B. G., DaRe, J. M., Kopcho, J. J., Browne, C. E., III, Schanzer, J. M., Wiesner, J. B., and Erion, M. D. (2000) Adenosine kinase inhibitors. 1. Synthesis, enzyme inhibition, and antiseizure activity of 5-iodotubercidin analogues. *J. Med. Chem. 43*, 2883–2893.
10. Vodnala, M., Fijolek, A., Rofougaran, R., Mosimann, M., Maser, P., and Hofer, A. (2008) Adenosine kinase mediates high affinity adenosine salvage in *Trypanosoma brucei*. *J. Biol. Chem. 283*, 5380–5388.
11. Parker, W. B., Barrow, E. W., Allan, P. W., Shaddix, S. C., Long, M. C., Barrow, W. W., Bansal, N., and Maddry, J. A. (2004) Metabolism of 2-methyladenosine in *Mycobacterium tuberculosis*. *Tuberculosis 84*, 327–336.
12. Wu, L. F., Reizer, A., Reizer, J., Cai, B., Tomich, J. M., and Saier, M. H., Jr. (1991) Nucleotide sequence of the *Rhodobacter capsulatus*

fruK gene, which encodes fructose-1-phosphate kinase: Evidence for a kinase superfamily including both phosphofructokinases of *Escherichia coli*. *J. Bacteriol. 173*, 3117–3127.
13. Holt, R. A., Subramanian, G. M., Halpern, A., Sutton, G. G., Charlab, R., Nusskern, D. R., Wincker, P., Clark, A. G., Ribeiro, J. M., Wides, R., Salzberg, S. L., Loftus, B., Yandell, M., Majoros, W. H., Rusch, D. B., Lai, Z., Kraft, C. L., Abril, J. F., Anthouard, V., Arensburger, P., Atkinson, P. W., Baden, H., de Berardinis, V., Baldwin, D., Benes, V., Biedler, J., Blass, C., Bolanos, R., Boscus, D., Barnstead, M., Cai, S., Center, A., Chaturverdi, K., Christophides, G. K., Chrystal, M. A., Clamp, M., Cravchik, A., Curwen, V., Dana, A., Delcher, A., Dew, I., Evans, C. A., Flanigan, M., Grundschober-Freimoser, A., Friedli, L., Gu, Z., Guan, P., Guigo, R., Hillenmeyer, M. E., Hladun, S. L., Hogan, J. R., Hong, Y. S., Hoover, J., Jaillon, O., Ke, Z., Kodira, C., Kokoza, E., Koutsos, A., Letunic, I., Levitsky, A., Liang, Y., Lin, J. J., Lobo, N. F., Lopez, J. R., Malek, J. A., McIntosh, T. C., Meister, S., Miller, J., Mobarry, C., Mongin, E., Murphy, S. D., O'Brochta, D. A., Pfannkoch, C., Qi, R., Regier, M. A., Remington, K., Shao, H., Sharakhova, M. V., Sitter, C. D., Shetty, J., Smith, T. J., Strong, R., Sun, J., Thomasova, D., Ton, L. Q., Topalis, P., Tu, Z., Unger, M. F., Walenz, B., Wang, A., Wang, J., Wang, M., Wang, X., Woodford, K. J., Wortman, J. R., Wu, M., Yao, A., Zdobnov, E. M., Zhang, H., Zhao, Q., Zhao, S., Zhu, S. C., Zhimulev, I., Coluzzi, M., della Torre, A., Roth, C. W., Louis, C., Kalush, F., Mural, R. J., Myers, E. W., Adams, M. D., Smith, H. O., Broder, S., Gardner, M. J., Fraser, C. M., Birney, E., Bork, P., Brey, P. T., Venter, J. C., Weissenbach, J., Kafatos, F. C., Collins, F. H., and Hoffman, S. L. (2002) The genome sequence of the malaria mosquito *Anopheles gambiae*. *Science 298*, 129–149.
14. Taylor, E. A., Rinaldo-Matthis, A., Li, L., Ghanem, M., Hazleton, K. Z., Cassera, M. B., Almo, S. C., and Schramm, V. L. (2007) *Anopheles gambiae* purine nucleoside phosphorylase: Catalysis, structure, and inhibition. *Biochemistry 46*, 12405–12415.
15. Darling, J. A., Sullivan, W. J., Jr., Carter, D., Ullman, B., and Roos, D. S. (1999) Recombinant expression, purification, and characterization of *Toxoplasma gondii* adenosine kinase. *Mol. Biochem. Parasitol. 103*, 15–23.
16. Tyler, P. C., Taylor, E. A., Frohlich, R. F., and Schramm, V. L. (2007) Synthesis of 5′-methylthio coformycins: Specific inhibitors for malarial adenosine deaminase. *J. Am. Chem. Soc. 129*, 6872–6879.
17. Sturm, M. B., and Schramm, V. L. (2009) Detecting ricin: Sensitive luminescent assay for ricin A-chain ribosome depurination kinetics. *Anal. Chem. 81*, 2847–2853.
18. Otwinowski, Z., and Minor, W. (1997) *Methods Enzymol. 276*, 307–326.
19. Vagin, A. A., and Teplyakov, A. (1997) *J. Appl. Crystallogr. 30*, 1022–1025.
20. Adams, P. D., Afonine, P. V., Bunkoczi, G., Chen, V. B., Davis, I. W., Echols, N., Headd, J. J., Hung, L. W., Kapral, G. J., Grosse-Kunstleve, R. W., McCoy, A. J., Moriarty, N. W., Oeffner, R., Read, R. J., Richardson, D. C., Richardson, J. S., Terwilliger, T. C., and Zwart, P. H. (2010) PHENIX: A comprehensive Python-based system for macromolecular structure solution. *Acta Crystallogr. D66*, 213–221.
21. Emsley, P., and Cowtan, K. (2004) Coot: Model-building tools for molecular graphics. *Acta Crystallogr. D60*, 2126–2132.
22. Murshudov, G. N., Vagin, A. A., and Dodson, E. J. (1997) Refinement of macromolecular structures by the maximum-likelihood method. *Acta Crystallogr. D53*, 240–255.
23. Laskowski, R. A., McArthur, M. W., Moss, D. S., and Thornton, J. M. (1993) *J. Appl. Crystallogr. 265*, 283–291.
24. Schumacher, M. A., Scott, D. M., Mathews, I. I., Ealick, S. E., Roos, D. S., Ullman, B., and Brennan, R. G. (2000) Crystal structures of *Toxoplasma gondii* adenosine kinase reveal a novel catalytic mechanism and prodrug binding. *J. Mol. Biol. 296*, 549–567.
25. Clements, A. N. (1992) The biology of mosquitoes, Vol. 1, Chapman and Hall, New York.
26. Knecht, W., Petersen, G. E., Sandrini, M. P., Sondergaard, L., Munch-Petersen, B., and Piskur, J. (2003) Mosquito has a single multisubstrate deoxyribonucleoside kinase characterized by unique substrate specificity. *Nucleic Acids Res. 31*, 1665–1672.
27. Miller, R. L., Adamczyk, D. L., Miller, W. H., Koszalka, G. W., Rideout, J. L., Beacham, L. M., III, Chao, E. Y., Haggerty, J. J., Krenitsky, T. A., and Elion, G. B. (1979) Adenosine kinase from rabbit liver. II. Substrate and inhibitor specificity. *J. Biol. Chem. 254*, 2346–2352.
28. Long, M. C., Escuyer, V., and Parker, W. B. (2003) Identification and characterization of a unique adenosine kinase from *Mycobacterium tuberculosis*. *J. Bacteriol. 185*, 6548–6555.
29. Zhang, Y., El Kouni, M. H., and Ealick, S. E. (2006) Structure of *Toxoplasma gondii* adenosine kinase in complex with an ATP analog at 1.1 angstroms resolution. *Acta Crystallogr. D62*, 140–145.
30. Zhang, Y., El Kouni, M. H., and Ealick, S. E. (2007) Substrate analogs induce an intermediate conformational change in *Toxoplasma gondii* adenosine kinase. *Acta Crystallogr. D63*, 126–134.
31. Muller, C. W., and Schulz, G. E. (1992) Structure of the complex between adenylate kinase from *Escherichia coli* and the inhibitor Ap_5A refined at 1.9 Å resolution. A model for a catalytic transition state. *J. Mol. Biol. 224*, 159–177.